

## **Update on Comparison of 2 mrad and 14 mrad Crossing Angle Extraction Lines at 0.5 GeV CMS**

**Ken Moffeit, Takashi Maruyama, Yuri Nosochkov, Andrei Seryi and  
Mike Woods**  
*SLAC*

**William P. Oliver**  
*Tufts University*

**Eric Torrence**  
*University of Oregon*

### **Abstract**

A study of the beam distributions in the 2 mrad and 14 mrad extraction lines are presented at beam energy of 250 GeV. Beam losses, energy losses due to synchrotron radiation and spin diffusion are shown. Synchrotron radiation distributions generated by the beam as it traverses the extraction lines are studied.

### **1. Introduction**

Two Interaction Regions (IR) are planned for the ILC. A possible configuration is to have one IR with a crossing angle of 14 /20 mrad and one with 2 mrad, as shown in Figure 1 [1]. MAD SURVEY file of the extraction beam optics was used to model the magnet locations, strengths, and orientations in GEANT [2]. Simulated disrupted beams from e+e- collisions for the ILC were transported using GEANT [2] in the extraction lines for the 2mrad and 14 mrad crossing angle interaction regions. Distributions of positions, energy and angles at (i) the middle of the Energy Chicane, (ii) at the Compton

IP for the measurement of polarization and (iii) at the Compton Detector Plane are shown. It is important to have small beam, energy and polarization losses between the Interaction Point and the Compton Polarimeter in the transport of the disrupted beam in the extraction lines. Beam losses, energy losses due to synchrotron radiation and spin diffusion are shown. Distributions of the synchrotron radiation are shown.

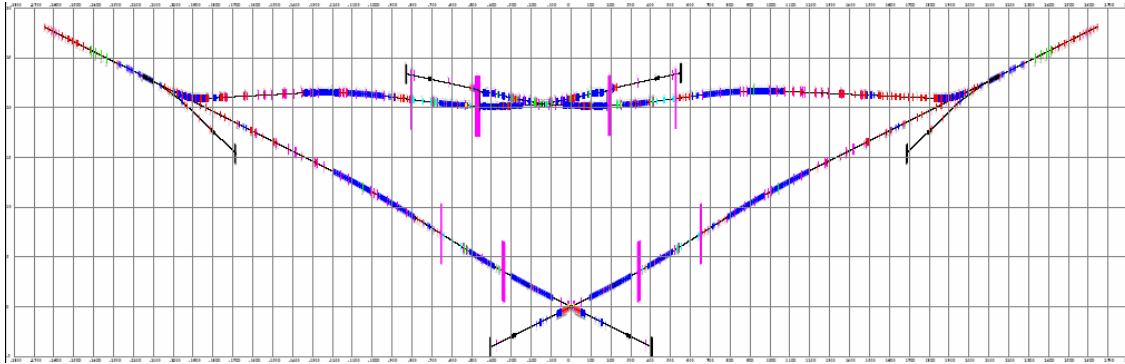


**Figure 1:** BDS layout. Grid size is 100m\*5m. Proposal for two IRs at the ILC. The electron and positron beams enter the final focus systems from the upper left and right. The IR at the top of the figure has the beams crossing at 2 mrad; the one at the bottom of the figure crosses at 14/20 mrad. A high resolution version of this figure can be found in Reference 3.

The 14 mrad IR allows the beam to continue straight ahead without bends in the horizontal plane. There are chicanes in the vertical plane for measuring the energy and polarization of the beam as shown in Figure 2. The beam is focused by quadrupoles at the Compton IP located at the center of the Polarimeter Chicane 147.682 meters downstream of the  $e^+e^-$  IR. The Energy Chicane is located between ~46m and 73m. Synchrotron radiation bands are generated by wiggler magnets in the horizontal plane when the beam has been directed along + or - 2 mrad by the bends in the vertical plane. Synchrotron radiation detectors are placed above and below the beam at the Compton IP to measure the separation between the horizontal bands and, as a result, the energy of the beam.

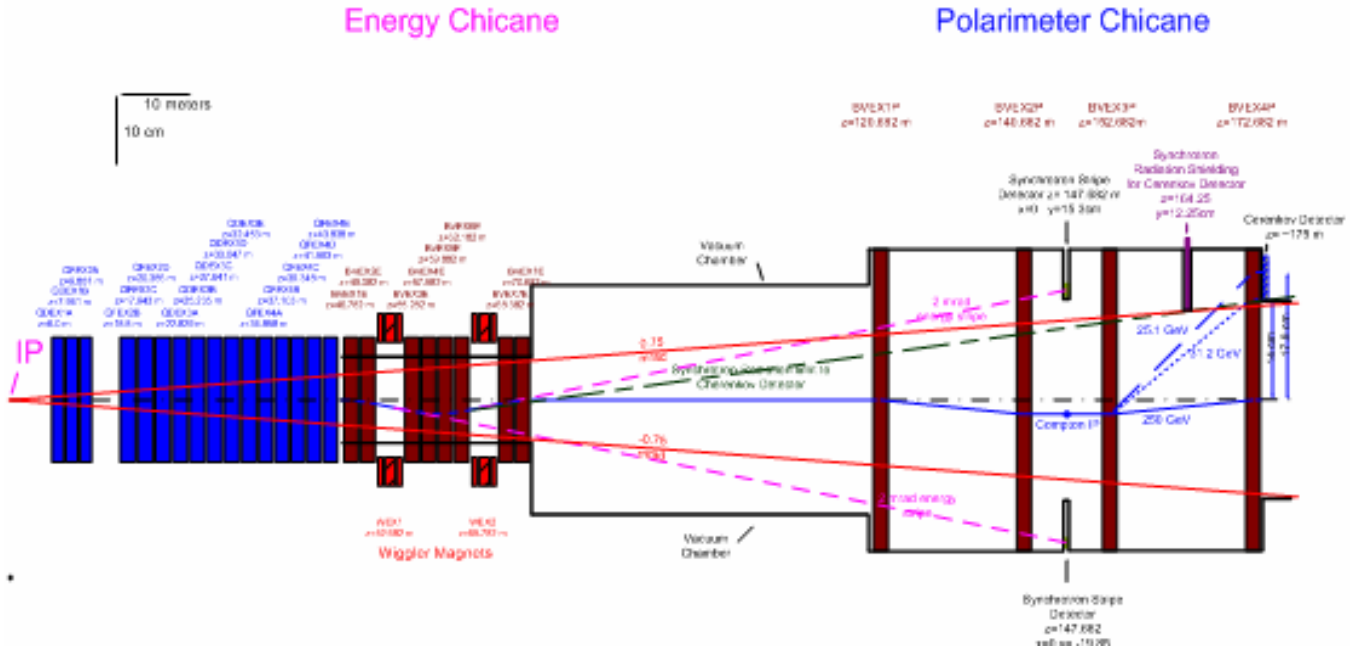


**Figure 2:** Diagram of the Energy Chicane and Polarimeter Chicane in the 14/20 mrad extraction line. Longitudinal distances are given from the IP. Also shown is the 0.75 mrad beam stay clear from the IP.

Figure 3 shows a schematic of the 2 mrad extraction line showing the plan view (top part of figure) and elevation view in the bottom portion of the figure. The 2mrad IR extraction line goes through the final focus magnets off axis, and the beam is extracted in the coil pocket of QF1 as shown in Fig. 4. This is necessary to separate the charged beam from the photons in the beamstrahlung cone of  $\pm 0.5$  mrad. The low energy beamstrahlung tail of the charged beam is absorbed by a series of collimators in the horizontal and vertical plane embedded in a vertical energy chicane. The Energy Chicane and the Polarimeter Chicane follow. Just before the Polarimeter Chicane the beam is bent back to the same direction it had at the e+e- IR. The direction of the beam at the Compton IP is required to be within 50 micro-radians of that at the e+e- IR, so that the polarization is the same as at the e+e- IR.



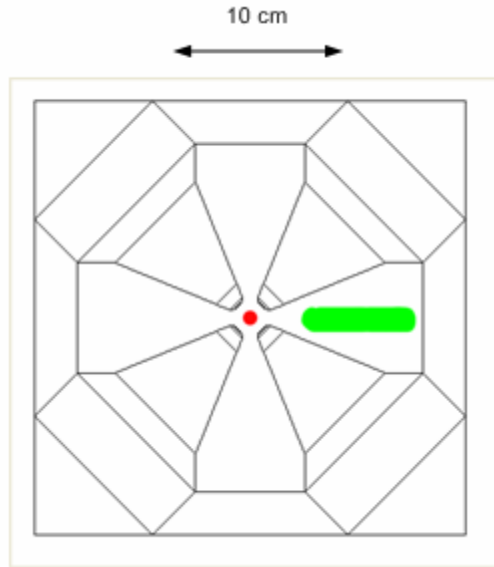


**Figure 4:** The figure shows QF1 for the 2mrad crossing angle extraction line. QF1 is special because it is a shared magnet by the incoming beam and the outgoing beam. The incoming beam is at the middle in red, and the outgoing disrupted beam is in the coil pocket in green.

The extraction line transport is simulated using the program GEANT[2]. Disrupted beam events were taken from files prepared by Andrei Seryi [4]. For these studies file cs11 corresponds to a normal ILC beam (mean energy 244.1 GeV and RMS 10.98 GeV), file cs13 with parameters set for large-y (mean energy 242.4 GeV and RMS 12.0 GeV) and file cs14 with parameters set for Low Power (234.6 GeV and RMS 22.10 GeV). The large-y parameter data sets are also shown for the centroid of the beams missing by 4nm (cs13  $dy = 4\text{nm}$ ) in the vertical (mean energy 241.9 GeV and RMS 12.48 GeV) and 200nm (cs13  $dx = 200\text{nm}$ ) in the horizontal (mean energy 242.7 GeV and RMS 11.81 GeV). Figure 5 shows a plot generated by GEANT giving the magnets and ray traces for 100 beam particles from the Normal ILC beam parameter data set. Figure 6 shows the energy distribution for the normal ILC beam parameters, cs11. Figure 7 shows the angular distributions of the disrupted beams for the different beam parameter sets as they leave the IR. The Low Power beam parameter data set has larger beam disruption resulting in broader energy and angular distributions.

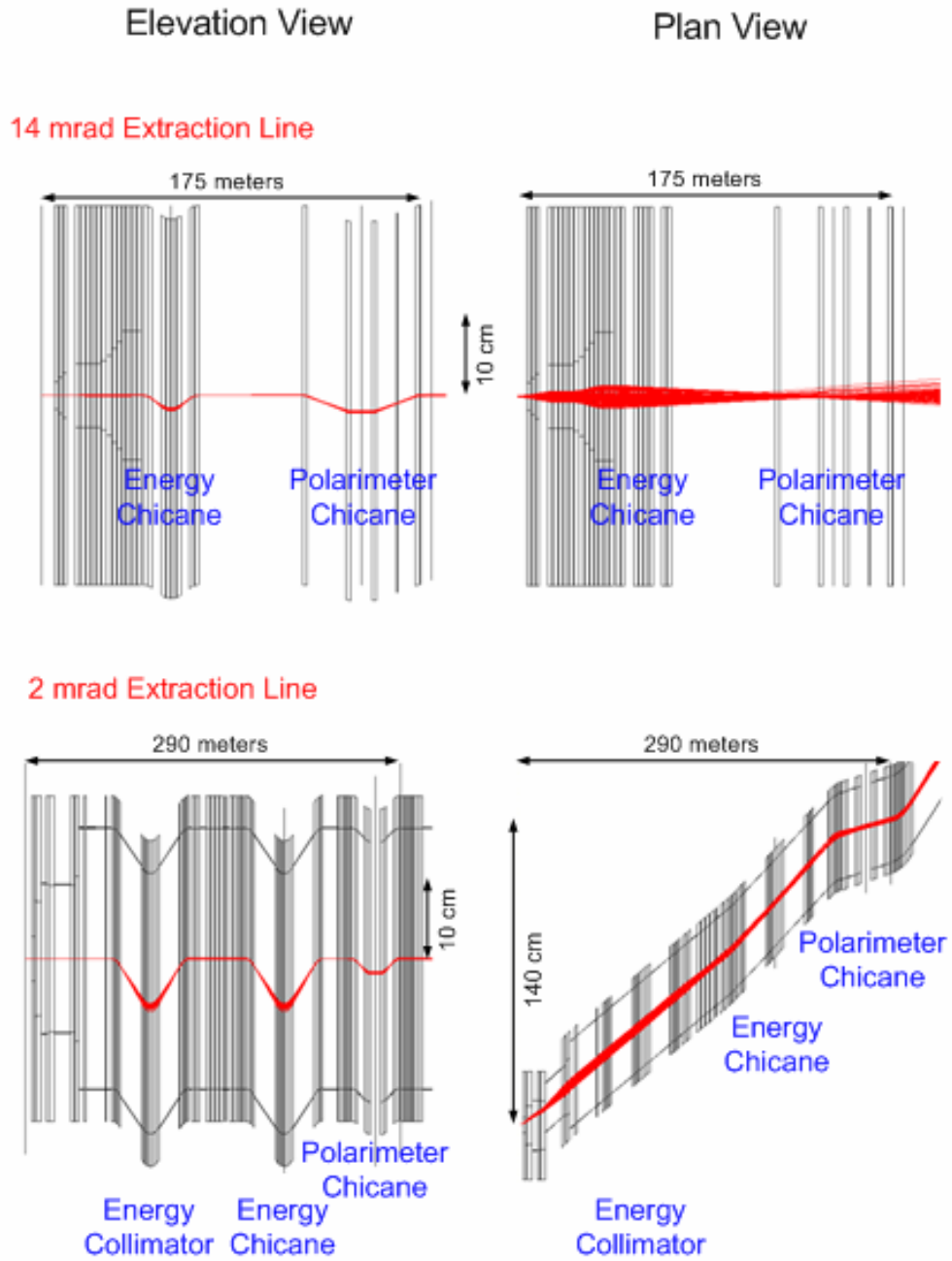


**Figure 5:** GEANT generated drawing of the beam line elements with 100 beam tracks shown.

## e+e- Interaction Region

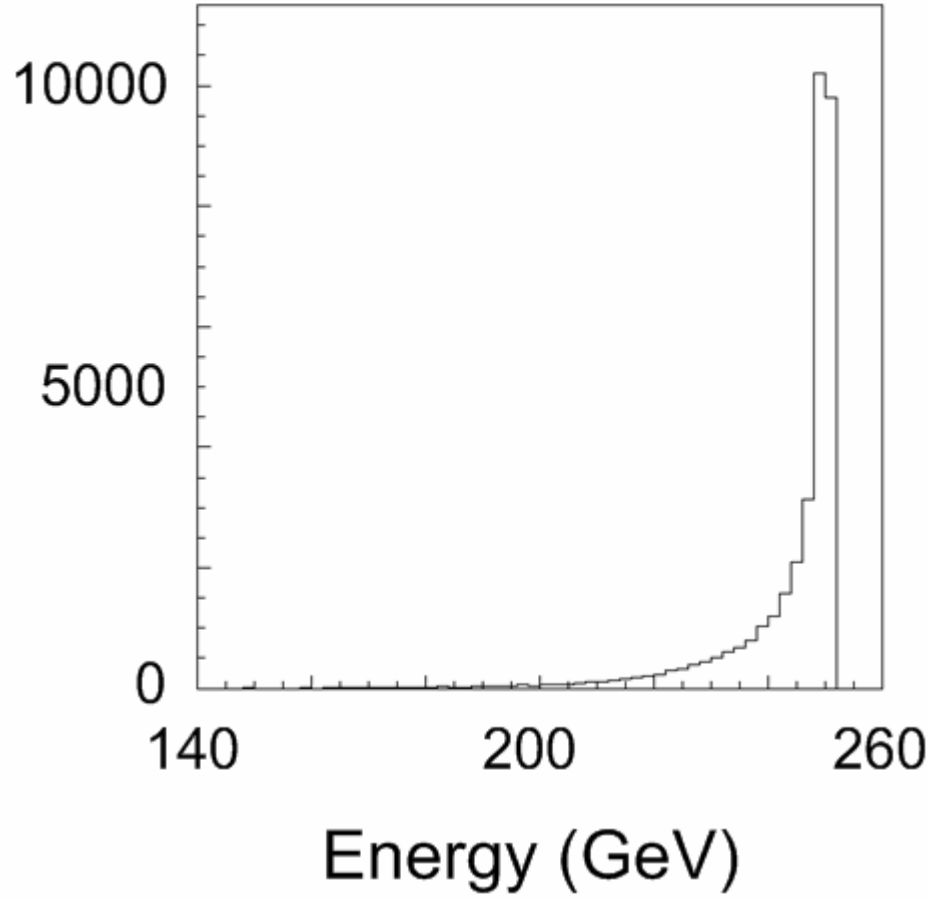


**Figure 6:** Energy distribution at the e+e- interaction region after collision for cs11 data set corresponding to a normal ILC beam [4].

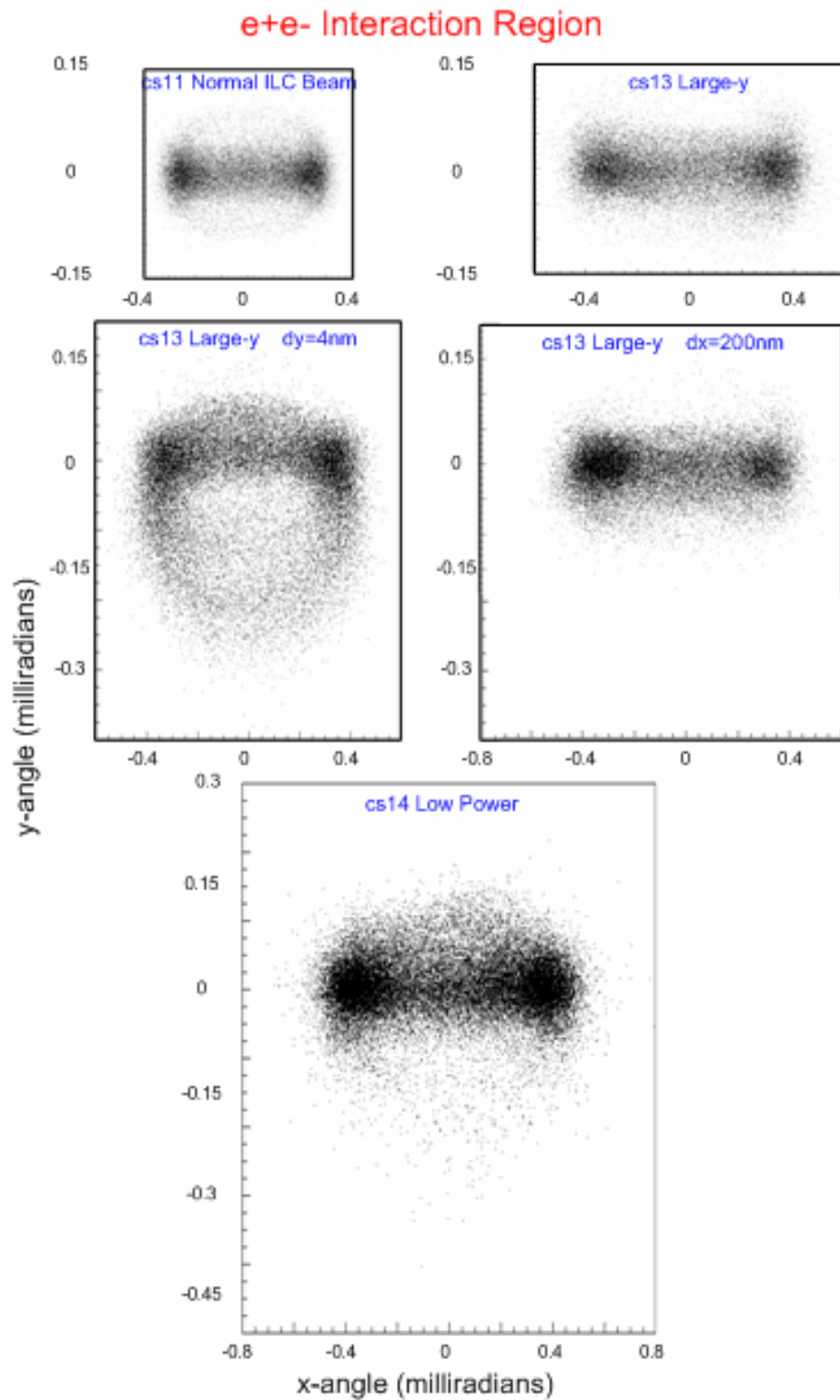


**Figure 7:** Angular distribution at the e+e- interaction region after collision for different data sets.

Beam distributions at the Compton IP are shown in figure 8. The tails of the beam spatial distributions and angular distributions are broader for the 2 mrad extraction line. The beam core distributions are also broader as seen in figure 9.

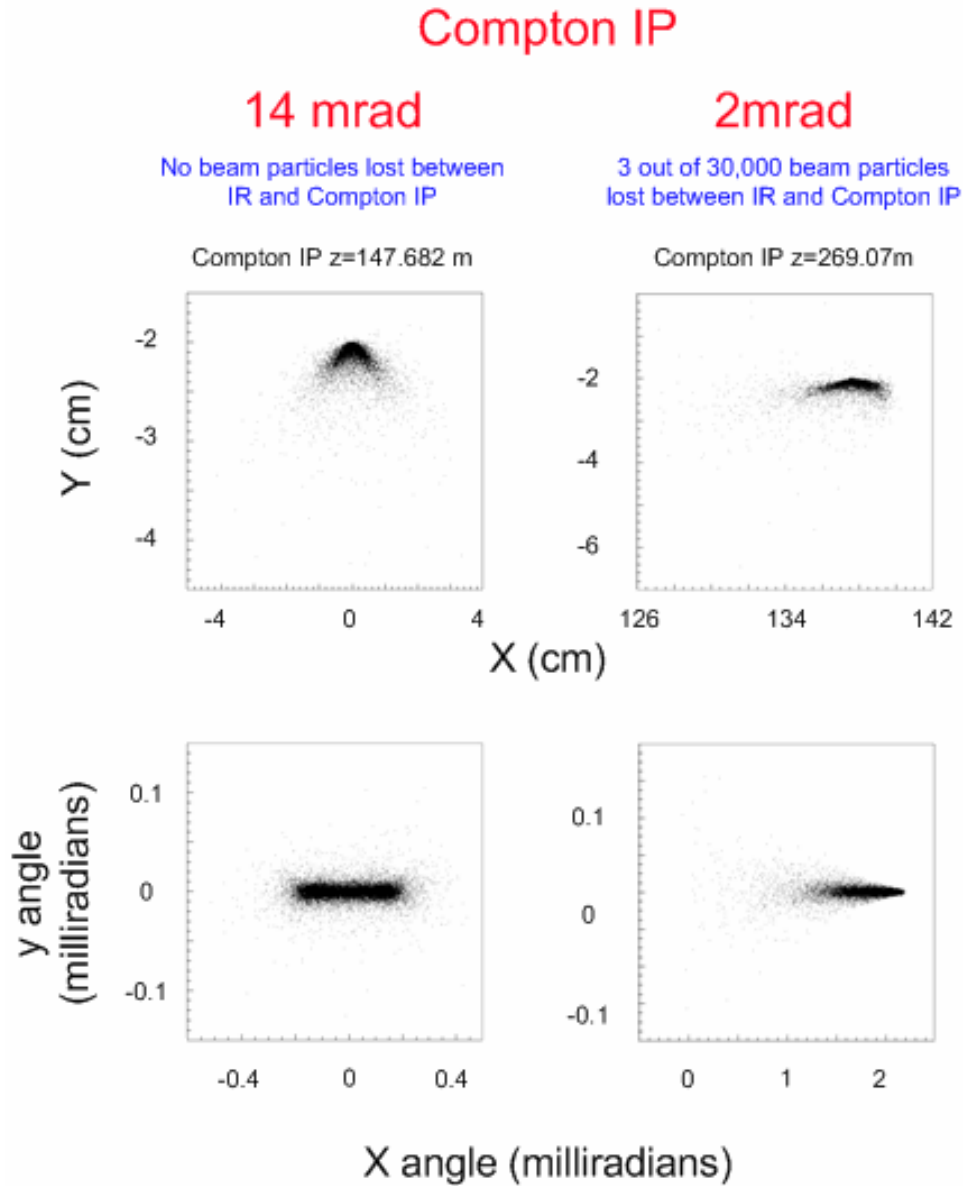


**Figure 8:** Distribution of y versus x and beam angles at the Compton IP for the 14 mrad and 2 mrad extraction lines. The dispersion at the Compton IP for particles of energy 250 GeV is -2cm.

## 2. Beam Distributions Contained within Laser Spot Size

The beam is much more diffuse at the Compton IP in the 2mrad extraction line than in the 14 mrad extraction line. This is seen in figure 9 where the distribution in x and y are given for those beam tracks within +/-100 microns of the peak. This corresponds to about the size of the laser spot at the Compton IP. The Compton luminosity is three times larger in the 14mrad extraction line than that of the 2mrad where the laser light sees only 14.7% of the beam.

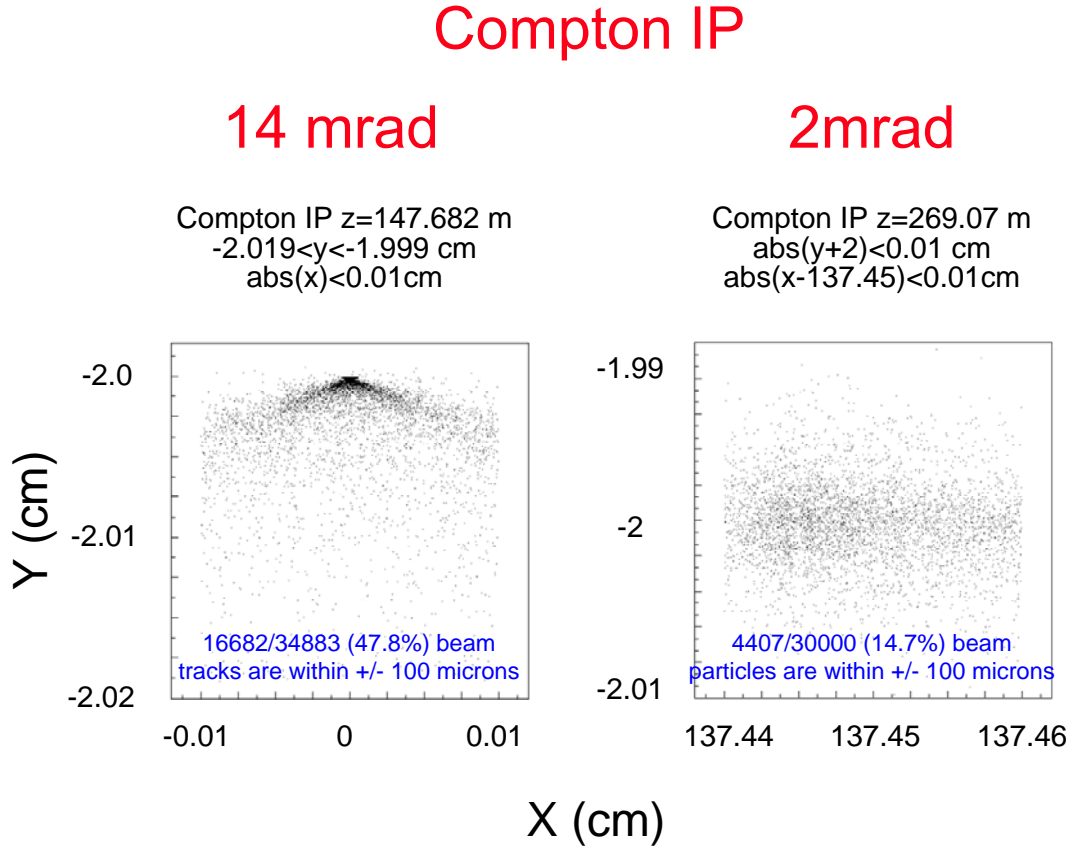


**Figure 9:** Distribution of y versus x within 100 microns of the peak at the Compton IP for the 14 mrad and 2 mrad extraction lines. The dispersion at the Compton IP for particles of energy 250 GeV is -2cm.

Spin Diffusion depolarization comes from classical (Bargmann-Michel-Telegdi precession: BMT) [5]. BMT spin precession with respect to the electron momentum vector is given by:

$$P = \cos(\theta_{spin}) = \cos\left(\gamma \frac{g-2}{2} \cdot \theta_{bend}\right) = \cos\left(\frac{E(\text{GeV})}{0.44065} \cdot \theta_{bend}\right) \quad (1)$$

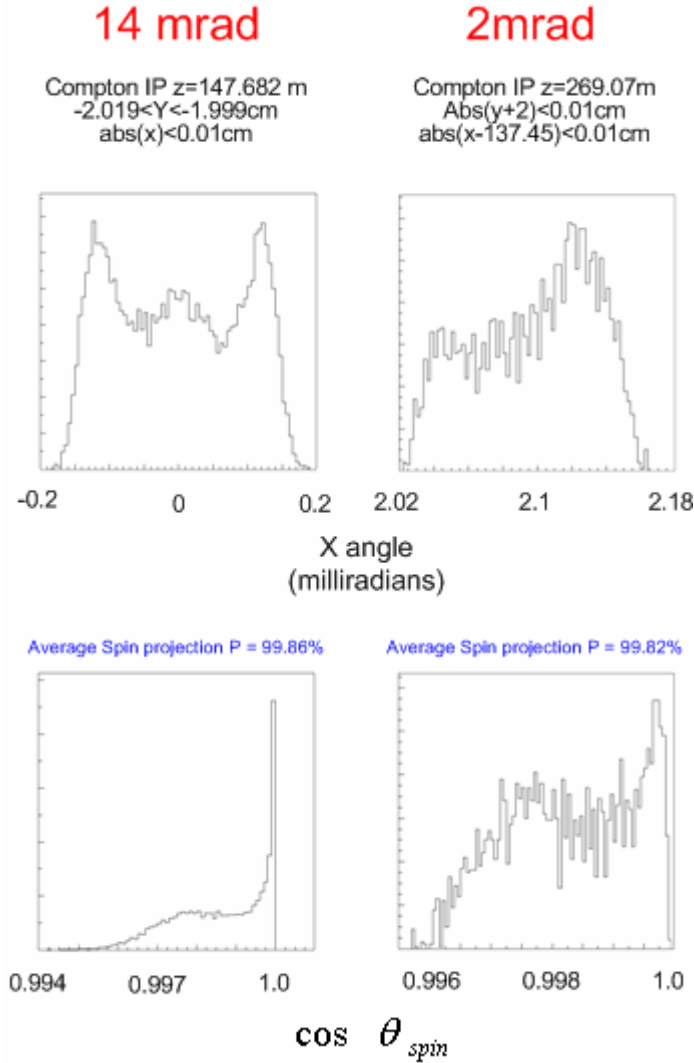
The change in spin direction for a bend angle change for electron beam energy of 250 GeV is 3.25 degrees for a directional change of 100 micro-radians and corresponds to a longitudinal polarization projection of 99.8%. When there is angular divergence of the beam greater than 100  $\mu$ rad there will be significant depolarization of the beam. As seen in Figure 10 the x-angle distribution at the Compton IP is contained within  $\pm 200$  micro-radians about the direction of the beam at the e+e- collision point. The y-angle distribution is much narrower than the x-angle distribution and does not contribute appreciable to the spin diffusion (see figure 8).

Figure 10 also shows the distribution of  $P = \cos(\theta_{spin})$  at the Compton IP. The mean is 99.86% for the 14mrad extraction line and 99.82% for the 2mrad extraction line distribution. The polarization at the Compton IP should be compared to the luminosity weighted polarization at the IR, which is approximated by:

$$P_{LuminosityWeighted} = \cos(\theta_{SpinLuminosityWeighted}) = \cos\left(\frac{E(GeV)}{0.44065} \cdot \frac{1}{2} \theta_{x-angle}^{IR}\right) \quad (2)$$

where  $\theta_{x-angle}^{IR}$  is the x-angle of the beam as it leaves the e+e- interaction region. As seen in Figures 7 the y-angle distribution at the IR is much narrower than the x-angle distribution and does not contribute appreciable to the spin diffusion. The polarization projection at the Compton IP is in excellent agreement with the luminosity weighted polarization of 99.84 % determined from equation 2. Note that the beam direction is 2mrad at the Compton IP for the 2 mrad IR extraction line and this has been subtracted from the angular distribution before taking the spin projection. Both extraction lines have small but not-negligible spin diffusion from the disrupted beam at the IR and the transport to the Compton IP.

The primary polarimeter measurement at the ILC will be performed by a Compton polarimeter. An accuracy of  $(P_{e^+} = P_{e^-}) = 0.25\%$  should be achievable [6]. Polarization measurements with collider data may reach an accuracy of 0.1% [6].



**Figure 10:** Angular distribution and  $\cos \theta_{spin}$  for beam particles within 100 microns of the peak at the Compton IP for the 14 mrad and 2 mrad extraction lines.  $\theta_{spin}$  is given by equation 1.

Table I gives the accepted beam and average polarization projection for various  $\pm 100$  micron selections about the x value of the beam at the Compton IP for the 2 mrad extraction line. The laser spot size at the Compton IP is  $\sigma \sim 100$  microns. Polarization is stable and the Compton luminosity decreases by a factor of four when moving off the peak by 600 microns. As can be seen in Figure 10 the x and y distributions fall off rapidly for the 14 mrad extraction line and only a few percent of the beam remains when stepping away from the peak.

**Table I: 2mrad Extraction Line:** Beam accepted and polarization projection for various  $\pm 100$  micron selections about the x value of the beam at the Compton IP. In each case  $\text{abs}(y+2.0\text{cm}) < 100$  microns and  $\text{abs}(x-137.45)$ .

<b>x <math>\pm</math> 100 microns</b>	<b>%Beam within <math>\pm</math> 100microns in x &amp; y</b>	<b>Luminosity Weighted Polarization at the IR</b>	<b>Polarization Projection</b>
137.45	14.7	99.84 %	99.82 %
137.47	6.0	99.84 %	99.89 %
137.49	4.8	99.84 %	99.94 %
137.51	3.8	99.84 %	99.94 %

Table II gives the beam accepted within  $\pm 100$  micro-meters about the peak at the Compton IP for different beam conditions at the IP. The Compton luminosity is decreased for the Large-y and Low Power beam parameter data sets. The 14mrad extraction line data shows the Compton Luminosity varies by  $< 10\%$  for the Large-y beam parameter data set when the beam collisions are offset by 200 microns in the horizontal and 4 microns in the vertical, while it changes by  $\sim 20\%$  for the 2 mrad extraction line.

The luminosity weighted polarization and the polarization projection at the Compton IP are also shown in Table II for the different data sets. The luminosity weighted polarization changes by 0.17 % between the Normal ILC beam parameter data set and the Low Power beam parameter data set. The Large-y and Low Power beam parameter data sets show small variation (less than 0.15%) between the polarization at the Compton IP and the luminosity weighted polarization.

The polarization measurement at the Compton IP should be within the desired precision of  $\pm 0.25\%$  for both the 2mrad and the 14 mrad extraction lines.

**Table II:** Beam accepted within  $\pm 100$  micro-meters about the peak and polarization projection for different data sets at the Compton IP.

**A) 14mrad Extraction Line with  $-2.019 < y < -1.999$ cm and  $\text{abs}(x) < 0.01$ cm:**

Condition (file name)	%Beam within $\pm 100$ microns in x & y	Luminosity Weighted Polarization at the IR	Polarization Projection
Nominal Beam Condition (cs11)	47.8	99.84 %	99.86 %
Large y (cs13)	34.7	99.68 %	99.74 %
Large y horizontal offset 200nm (cs13_dx200)	35.3	99.68 %	99.73 %
Large y vertical offset 4nm (cs13_dy4)	32.0	99.72 %	99.74 %
Low Power (cs14)	28.4	99.67 %	99.69 %

**B) 2 mrad Extraction Line with  $\text{abs}(y+2) < 0.01$ cm and  $\text{abs}(x-137.45) < 0.01$ cm:**

Condition (file name)	%Beam within $\pm 100$ microns in x & y	Luminosity Weighted Polarization at the IR	Polarization Projection
Nominal Beam Condition (cs11)	14.5	99.84 %	99.82
Large y (cs13)	6.9	99.68 %	99.83
Large y horizontal offset 200nm (cs13_dx200)	8.2	99.68 %	99.81
Large y vertical offset 4nm (cs13_dy4)	5.6	99.72 %	99.82
Low Power (cs14)	5.0	99.67 %	99.81

### 3. Beam Losses

Beam losses between the Interaction Region and the Compton Detector Plane are given in Table III. The 14mrad extraction line had no losses in 34,883 beam particles for the Normal ILC and Large-y beam parameter conditions. The losses are  $1.1 \cdot 10^{-4}$  for the

Low Power beam parameter data set. The losses are larger for the 2mrad crossing angle extraction being more than  $1.3 * 10^{-4}$  of the beam for the Normal ILC beam parameter data set. The Low Power beam parameter data set has losses of 1.25%.

**Table III:** Beam Losses from the e+e- IR to the Compton Detector Plane.

**a) 14 mrad Crossing Angle Extraction Line**

Condition (file name)	Losses	Beam	Lost Beam
Normal ILC Beam Condition (cs11)	0	34883	$<0.5 * 10^{-4}$
Large y (cs13)	0	34907	$<0.5 * 10^{-4}$
Large y horizontal offset 200nm (cs13_dx200)	0	34898	$<0.5 * 10^{-4}$
Large y vertical offset 4nm (cs13_dy4)	0	34923	$<0.5 * 10^{-4}$
Low Power (cs14)	4	34913	$1.1 * 10^{-4}$

**b) 2 mrad Crossing Angle Extraction Line**

Condition (file name)	Losses	Beam	Lost Beam
Nominal Beam Condition (cs11)	5	34883	$1.4 * 10^{-4}$
Large y (cs13)	32	34907	$9.2 * 10^{-4}$
Large y horizontal offset 200nm (cs13_dx200)	32	34898	$9.2 * 10^{-4}$
Large y vertical offset 4nm (cs13_dy4)	29	34923	$8.3 * 10^{-4}$
Low Power (cs14)	437	34913	$125 * 10^{-4}$

Beam losses were further studied by using a file with the tails of the disrupted beam having events with energy less than 0.65 of the beam energy or the angle greater than 0.5 mrad:

[http://www.slac.stanford.edu/~seryi/ILC\\_new\\_gp\\_files/cs11\\_hs/taill1\\_lt\\_0\\_65E0\\_or\\_gt\\_500urad.dat](http://www.slac.stanford.edu/~seryi/ILC_new_gp_files/cs11_hs/taill1_lt_0_65E0_or_gt_500urad.dat)

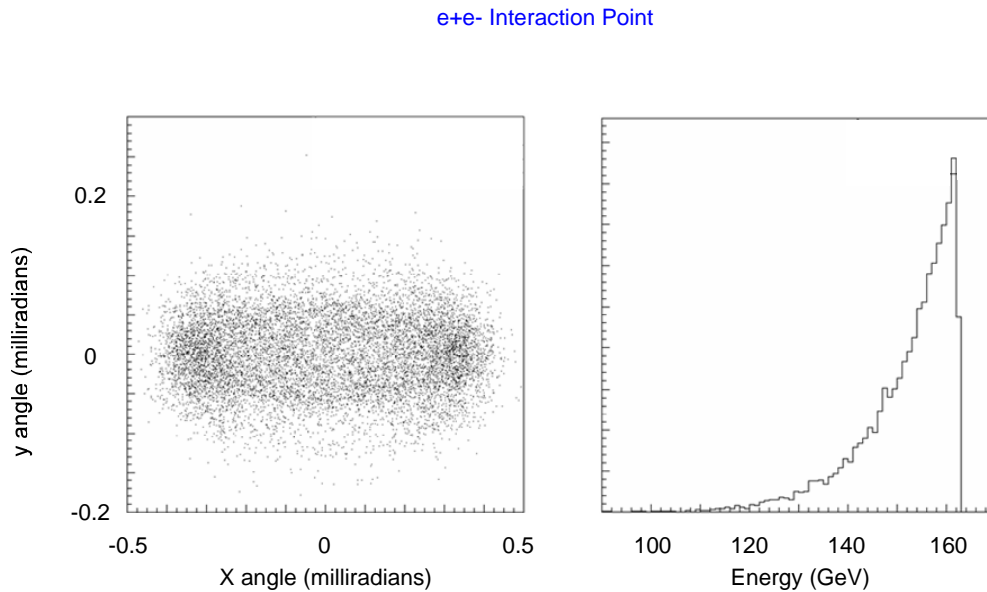
Figure 11 shows the energy and angular distributions of the 10,503 disrupted beam tracks from the 17.59 million original beam tracks. All the events are contained within 0.5 mrad, so, only the energy selection contributes to the tail sample.

No particles from this tail sample are lost in the 14 mrad extraction giving a loss of less than  $10^{-7}$ .

The 2 mrad extraction has large losses. There are major collimation losses of the beam tails particularly at  $z=119\text{m}$  and  $z=156\text{m}$ . Only 5899 of the 10,503 particles continue to the Compton Detector plane. This represents a loss of  $2.62 * 10^{-4}$  of the 17.59 million original beam tracks. Figure 12 shows the x and y distributions at the Compton Detector plane. There is significant background in the region of the Compton Cherenkov Detector coming mainly from secondary photons. From this study we estimate  $\sim 50$

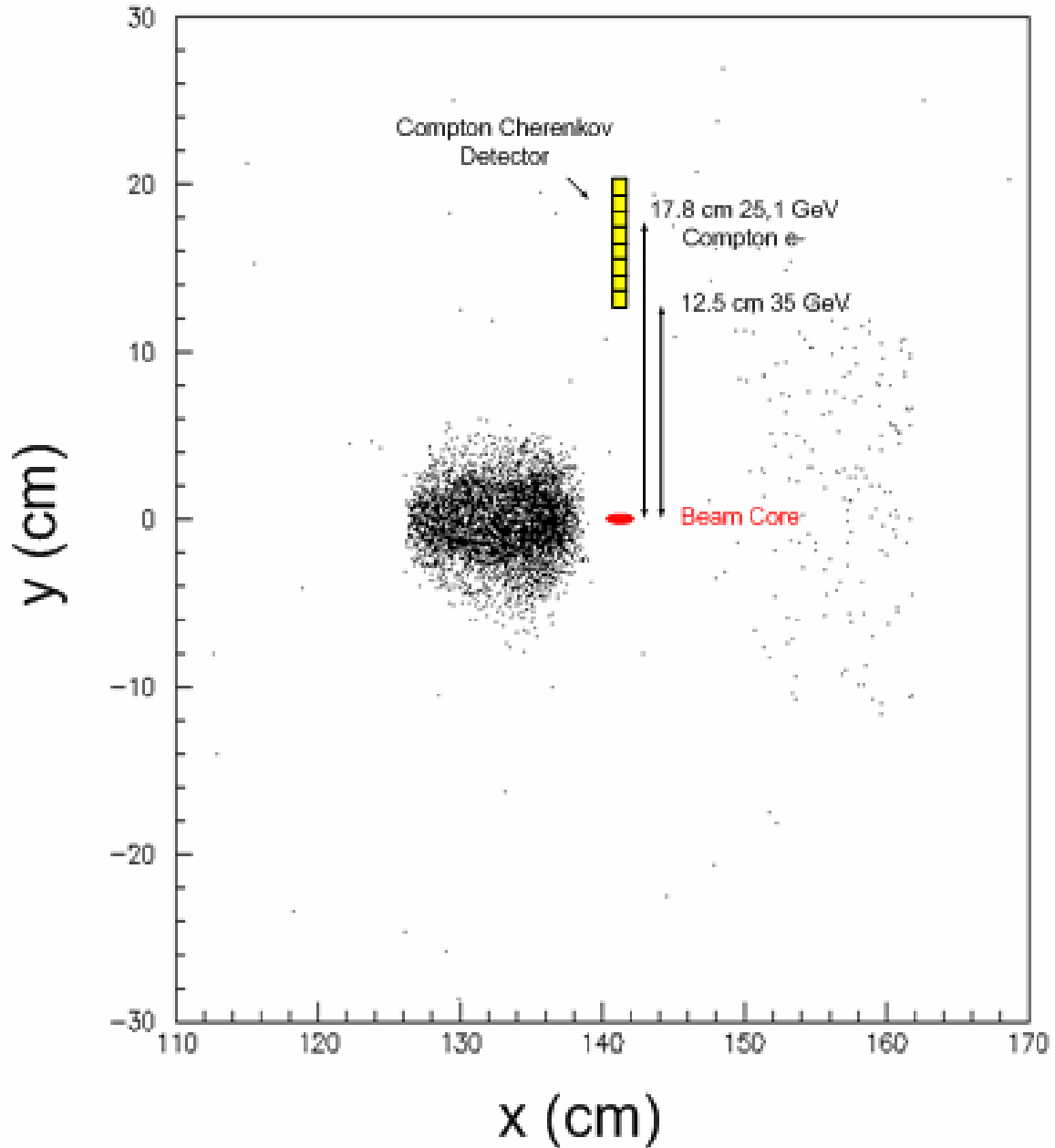
photons/cm<sup>2</sup> are in the region of the Cherenkov counter cells for each bunch of  $2 \cdot 10^{10}$  electrons. The energy spectrum of the secondary photons is peaked at low energy with only ~20% above 10 MeV (threshold for an electron to give Cherenkov light is ~10 MeV). Local shielding of the Cherenkov detector cells will be necessary to reduce the background from secondary photons and charged particles. The backscattered electron counting rate is high for the proposed Compton Polarimeter with about 650 Compton electrons per GeV at the endpoint energy of 25.1 GeV, which would correspond to more than a 1000 Compton electrons per 1 cm Cherenkov cell [7]. Therefore the backgrounds from secondary interactions should be small compared to the signal.

The Low Power beam parameter data set shows very large backgrounds in the region of the Cherenkov detector for the 2 mrad extraction line. There are an estimated  $\sim 4 \cdot 10^4$  photons per cm<sup>2</sup> at the Cherenkov detector with ~20% having energy above Cherenkov threshold.



**Figure11:** 2mrad Extraction Line: Tail sample angular and energy distributions at the e+e- interaction point for outgoing beam particle with energy less than 0.65 of the incoming beam energy or angles greater than 0.5 mrad. There were 17.59 million beam particles used to generate these 10503 tail beam particles.

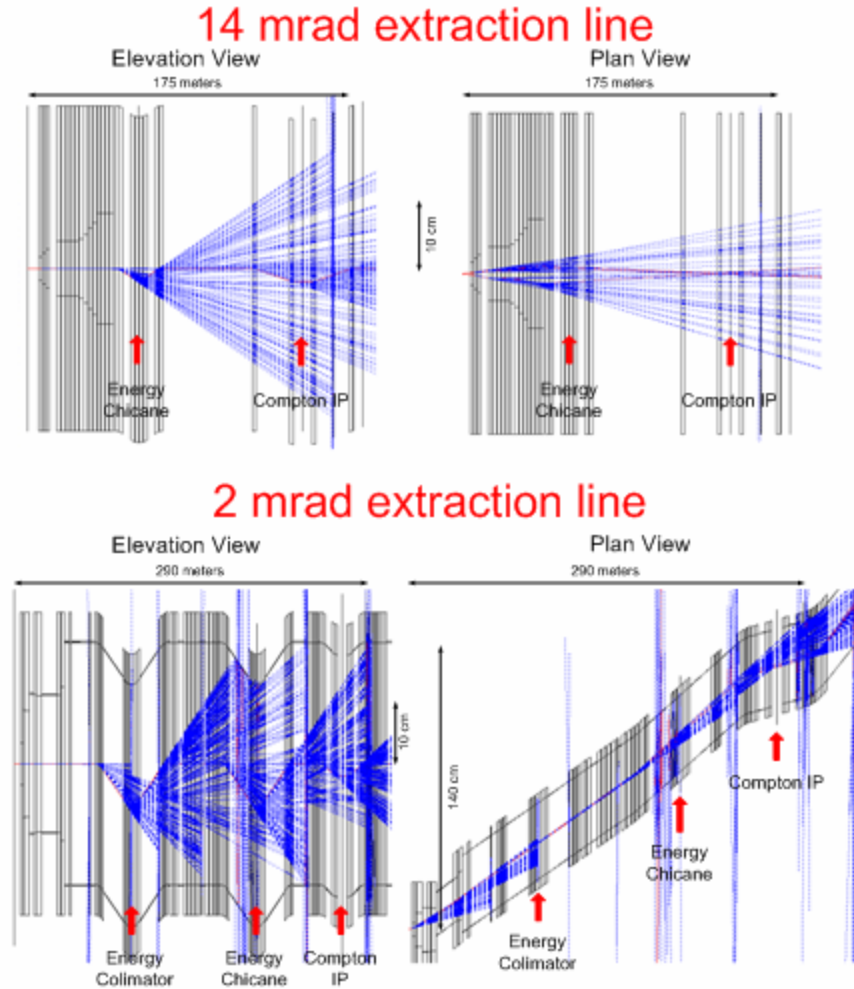
# Compton Detector Plane $z=288.37$ m



**Figure12:** *2 mrad extraction line:* The horizontal and vertical distributions of the tail sample at the Compton Detector plane of the beam particles and background produced from the lost beam particles.

## 4. Synchrotron Radiation

Synchrotron radiation is produced in the bends and quadrupole magnets and is shown by the blue rays in figure 13. Due to the horizontal bends and the energy collimator chicane in the 2 mrad extraction more synchrotron radiation is generated.



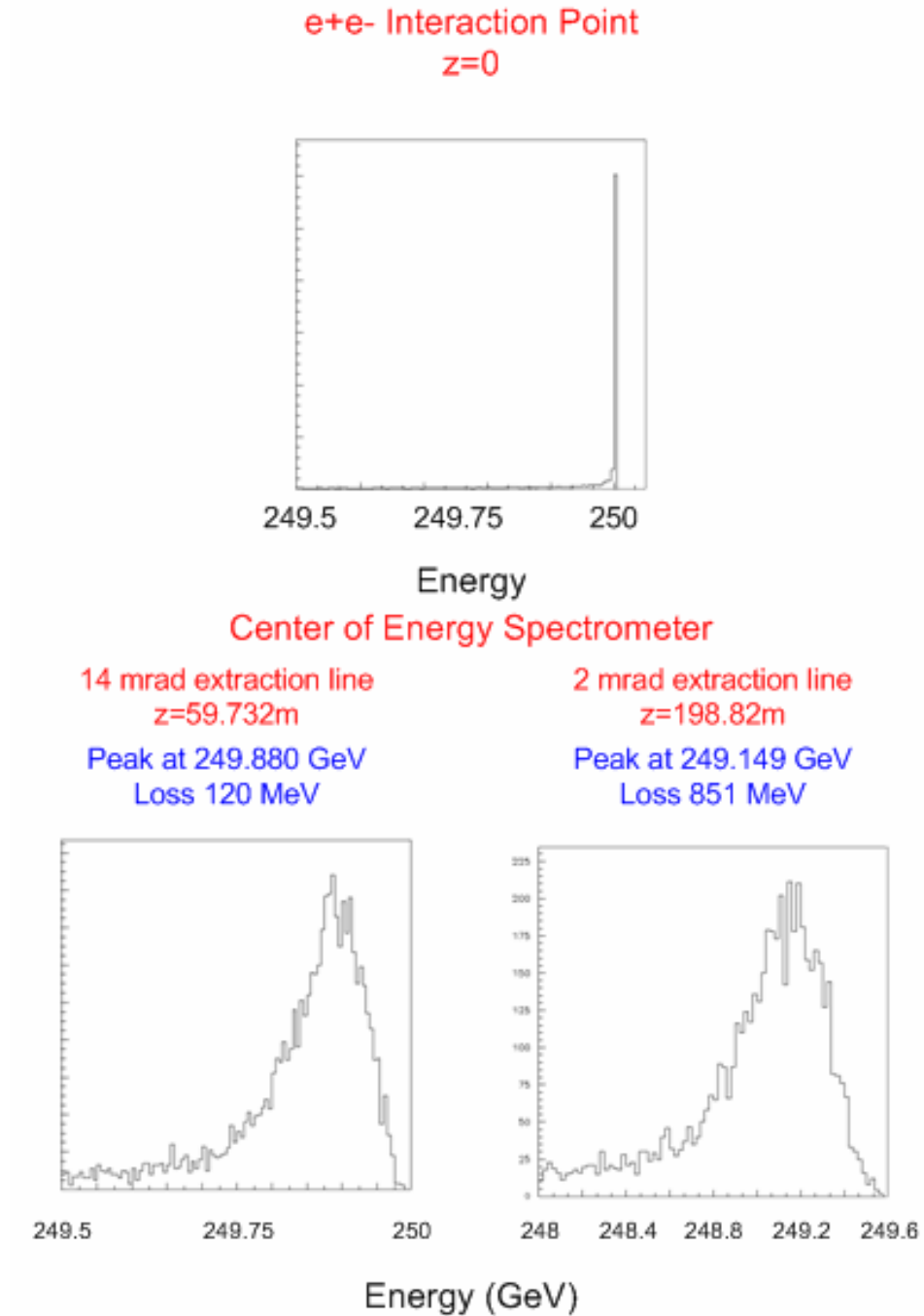
**Figure 13:** Synchrotron radiation in the 14 mrad and 2 mrad extraction lines. The rays colored blue are the synchrotron radiation rays.

Figure 14 shows the energy of the beam at the  $e^+e^-$  interaction point and at the middle of the energy spectrometer for the 14 mrad and 2 mrad extraction lines. At the  $e^+e^-$  interaction point there is a long beamstrahlung tail with about a third of the beam in the peak at 250 GeV. Synchrotron radiation losses broaden the peak and shift it to a lower energy. Beam energy losses due to synchrotron radiation between the Interaction Region and the center of the Energy Chicane are given in Table IV for the different disrupted

beam parameter sets. An energy loss of  $\sim 120$  MeV occurs in the 14 mrad extraction line with variation between beam parameter data sets of less than 6 MeV. Selecting beam particles with  $E > 240$  GeV gives synchrotron radiation losses larger by a few MeV reflecting the higher energy of the beam particles selected. The energy spectrometer will measure the distributions of energy in the lower part of figure 14.

The 2 mrad extraction line has larger energy losses of  $\sim 850$  MeV. The variation between beam parameter data sets is partly due to the broader energy spectrum in the Large-y and Low Power beam parameter data sets and to changes in the path of the beam in the horizontal plane seeing different magnetic fields going through the quadrupoles off axis. Selection beam tracks near the peak energy ( $E > 240$  GeV) results in a small variation in the energy loss with beam condition except for the Large-y beam parameter data set with the beams missing by 200nm in the horizontal plane. Here the energy loss is  $\sim 25$  MeV lower than the other data sets.

It is important to know the energy at the  $e^+e^-$  interaction point to a precision of  $\sim 25$  MeV. The large synchrotron radiation losses between the  $e^+e^-$  interaction point and the energy spectrometer in the 2 mrad extraction line will have to be understood to that level. A beam collision offset in the horizontal plane causes variation of the energy loss due to synchrotron radiation similar to the measurement precision goal of 25 MeV.



**Figure 14:** Energy of the disrupted beam at the e+e- interaction point and at the center of the energy spectrometer for the 14 mrad ( $z=59.732\text{m}$ ) and 2 mrad ( $z=198.82\text{m}$ ) extraction lines. The lower energy of the peak is due to synchrotron radiation losses in the magnets.

**Table IV: Energy Loss due to synchrotron radiation.** Energy at the e+e- IR minus the energy at the Center of the Energy Chicane for all beam tracks and for those with E>240GeV.

**a) 14 mrad Crossing Angle Extraction Line**

Condition (file name)	Energy Loss (MeV)	Energy Loss (MeV) for E>240GeV
Nominal Beam Condition (cs11)	117	120
Large y (cs13)	121	125
Large y horizontal offset 200nm (cs13_dx200)	121	124
Large y vertical offset 4nm (cs13_dy4)	121	125
Low Power (cs14)	117	126

**b) 2 mrad Crossing Angle Extraction Line**

Condition (file name)	Energy Loss (MeV)	Energy Loss (MeV) for E>240GeV
Nominal Beam Condition (cs11)	829	851
Large y (cs13)	831	852
Large y horizontal offset 200nm (cs13_dx200)	806	827
Large y vertical offset 4nm (cs13_dy4)	832	854
Low Power (cs21)	802	862

The x vs y distribution of the synchrotron radiation at the Compton IP is shown in figure 15. The location of the synchrotron radiation from the wigglers is shown by the yellow bars (synchrotron radiation from the wigglers are not simulated in this study). The horizontal offset seen in the 2 mrad extraction line is due to the horizontal bend between the energy spectrometer and the Compton IP. The strength of the wiggler bend angle will be chosen so that the synchrotron radiation stripe detectors will not be sensitive to most of the background from the main bend stripe, and good signal to noise will be achievable.

## Compton IP

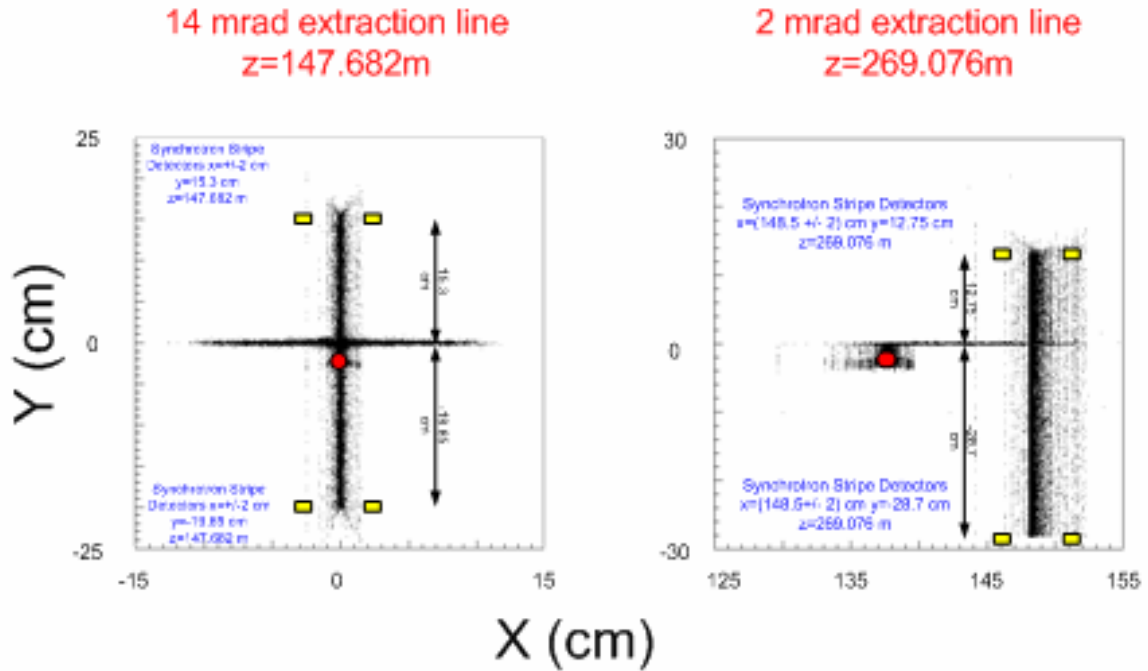


**Figure 15:** The x vs y distribution of the synchrotron radiation at the Compton IP for the 14 mrad extraction line and the 2 mrad extraction line. The yellow bars show the location of the synchrotron radiation from the wigglers of the energy spectrometer (not generated in this GEANT study).

The synchrotron radiation is shown in figure 16 at the location of the Compton Detector. Due to the horizontal bends in the 2 mrad extraction line the Compton detector does not see the direct synchrotron radiation from the upstream magnets. However, there are scattered synchrotron radiation photons in the region of the Cherenkov Detector. From a study of 10,000 beam tracks there is an estimated  $0.6 \cdot 10^6$  photons per  $\text{cm}^2$  per  $2 \cdot 10^{10}$  beam particles in the region of the Cherenkov Detector. The photon energy spectrum is at low energy mainly below Cherenkov threshold. It is important to design the collimation with this in mind and to properly shield the detector.

This is different for the 14 mrad extraction line. A collimator needs to be placed at  $z \sim 164.25\text{m}$  in the 14 mrad extraction line to intercept the synchrotron radiation above the 0.75 mrad beam stay clear (12.25cm). As seen in figure 16 the first Cherenkov cell beginning at  $y \sim 14$  cm does not see the direct synchrotron radiation, which is below 13.7 cm. It may be necessary to begin the first Cherenkov cell higher than 14 cm or extend the collimator at  $z \sim 164.25\text{m}$  slightly inside the 0.75 mrad beam stay clear. Compton backscattered electrons of 31.2 GeV will reach the Compton detector at  $y = 14$  cm. Compton scattering at 180 degrees has electron energy of 25.1 GeV and reaches the Compton detector at  $y = 17.8$  cm. Four 1 cm Cherenkov cells can cover the range of the

Compton scattering between the beam pipe and the kinematic edge. In a study of 10,000 beam tracks only 1 photon is above  $y=14$  cm. Care should be taken to design the collimator at  $z=164.25$  m so that synchrotron radiation photons do not rescatter into the direction of the Cherenkov counter.

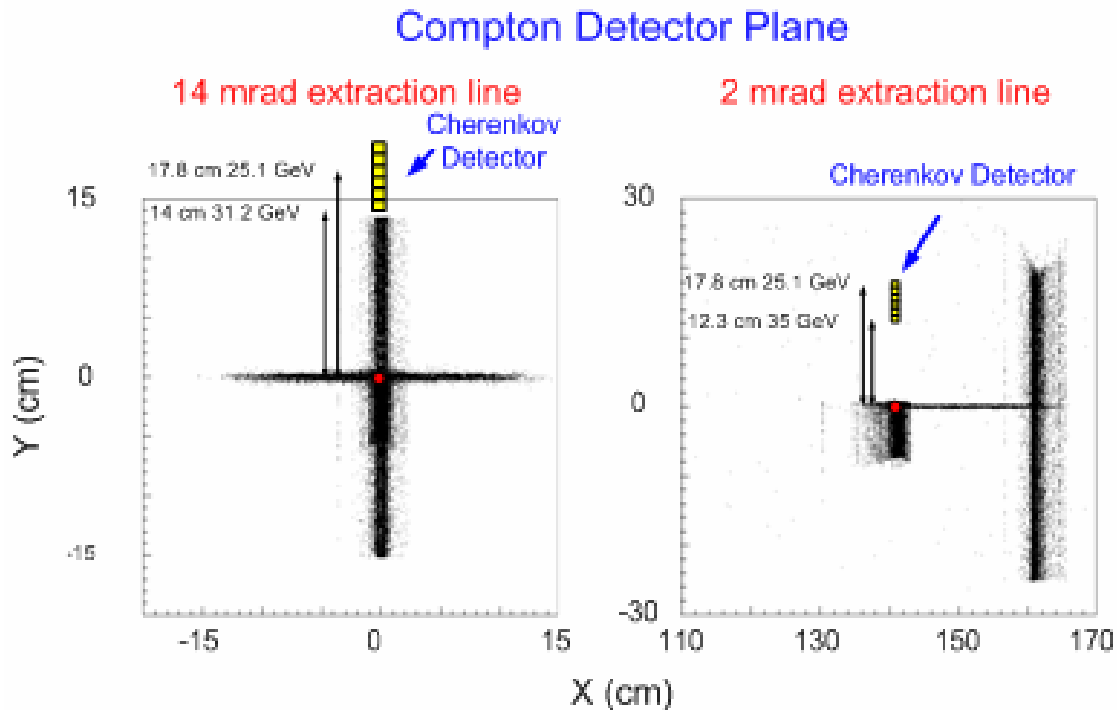


**Figure 16:** The x vs. y distribution of the synchrotron radiation at the Compton Detector for the 14 mrad extraction line and the 2 mrad extraction line. The yellow bars show the location of the Cherenkov detector.

## 5. Conclusions

The 14 mrad extraction line:

- At the Compton IP 48% of the beam is contained within  $\pm 100$  microns of the peak giving reasonable luminosity for Compton scattering of the laser light on the disrupted electron beam.
- The polarization projection at the Compton IP is in good agreement with the luminosity weighted polarization at the  $e^+e^-$  interaction region. A precision measurement of  $\pm 0.25\%$  will be possible.

- No beam losses from e+e- IR to Compton detector plane out of 17.6 million beam tracks for the Normal ILC and the Large-y beam parameter data set. The Low Power beam parameter data set has losses of  $1.1 * 10^{-4}$ .
- Beam energy loss due to synchrotron radiation between the e+e- IR and the middle of energy chicane (z=59.7 m) is only ~120 MeV and shows small variations of less than 10 MeV with different beam parameter conditions for the disrupted beam.
- The collimator at z=164.25 meters needs to be designed. It absorbs the synchrotron radiation above the 0.75 mrad beam stay clear allowing the Cherenkov detector to begin at y~14 cm.

The 2 mrad extraction line:

- There are large beam losses for the Normal ILC beam parameter data set between the e+e- IR and Compton detector plane ( $>2.6*10^{-4}$  are lost) giving secondary backgrounds of mainly photons in the region of the Cherenkov Detector. The Low Power beam parameter data set has beam losses ~ 1.25% giving very large backgrounds at the Cherenkov detector.
- A small percentage of the beam is hit by laser spot +/-100 microns (~15%) at the Compton IP and results in low Compton luminosity.
- The polarization projection at the Compton IP is in good agreement with the luminosity weighted polarization at the e+e- interaction region. A precision measurement of +/-0.25% will be possible.
- There are large beam energy losses (~850 MeV) due to synchrotron radiation between IR and the center of the energy chicane at z=198.82 meters. Beam collision jitter in the horizontal plane of 200 nanometers gives changes in the beam energy loss due to synchrotron radiation of ~25 MeV comparable to the goal of the precision measurement of the energy.
- Synchrotron radiation at the Cherenkov Detector is favorable. However, there are scattered synchrotron radiation photons in the region of the Cherenkov Detector. The photon energy spectrum is at low energy mainly below Cherenkov threshold. It is important to design the collimation with this in mind and to properly shield the detector.

## References

[1] Workshop on Machine-Detector Interface at the International Linear Collider, Andrei Seryi et al., Crossing Angle Session, see <http://www-conf.slac.stanford.edu/mdi/>, talk by R. Appleby, talk by Y. Nosochkov, [Extraction Line Designs for 2mrad and 20mrad IRs](#), figure 1 from Andrei Seryi “Tunnel layout, underground space and access requirements in BDS”, 30 April 2006.

Optics of the ILC extraction line for 2 mrad crossing angle.

Y. Nosochkov, K. Moffeit, A. Seryi, C. Spencer, M. Woods (SLAC), D. Angal-Kalinin, R. Appleby (Daresbury), B. Parker (Brookhaven).  
SLAC-PUB-11613, EUROTEV-REPORT-2006-001, SNOWMASS-2005-ILCAW0525, Jan 2006.

ILC Extraction Line for 14 mrad Crossing Angle.

Y. Nosochkov, T. Markiewicz, T. Maruyama, A. Seryi (SLAC), B. Parker (Brookhaven).  
SLAC-PUB-11591, Dec 8, 2005.

[2] GEANT-3, CERN Program Library Long Write-up W5013, CERN, March 1994.

[3] A high resolution version of Figure 1 can be found at: [http://www-project.slac.stanford.edu/ilc/acceldev/beamdelivery/rdr/components/ILC2006b\\_BDS\\_layout.pdf](http://www-project.slac.stanford.edu/ilc/acceldev/beamdelivery/rdr/components/ILC2006b_BDS_layout.pdf)

[4] Andrei Seryi, <http://www.slac.stanford.edu/~seryi/>, November 2005.

[5] V. Bargmann, L. Michel, and V.L. Telegdi. *Precession of the polarization of particles moving in a homogeneous electro-magnetic field*. *Phys. Rev. Lett.* 2(10):435-436, 1959.

[6] G. Mootgat-Pick, et al., *The role of polarized positrons and electrons in revealing fundamental interactions at the Linear Collider*, SLAC-PUB-11087, May 2005.

[7] Ken Moffeit and Mike Woods, *Laser System for a Compton Polarimeter*, IPBI TN-2003-2, December 2003,

<http://www.slac.stanford.edu/xorg/lcd/ipbi/notes/ComptonLaserSystem.pdf>